KnE Engineering

Knowledge E
enriching | engaging | empowering

Conference Paper

Cadastral Surveys with Non-metric Camera Using Uav: A Feasibility Study

Catur A. Rokhmana[1], Martinus E. Tjahjadi[2], and Fransisca D. Agustina[2]

[1]Department of Geodetic Engineering, Gadjah Mada University, Indonesia
[2]Department of Geodesy, National Institute of technology (ITN Malang), Indonesia

Corresponding Author:
Catur A. Rokhmana
caris@ugm.ac.id

OPEN ACCESS

Abstract

Orthophoto maps are believed by mapping communities as a favorable media to generate land parcel boundaries for cadaster survey related projects. However, since burgeoning off-the-shelf cameras mounted on the unmanned aerial vehicle (UAV) are commonly utilized for photographing such boundaries, unreliable and unstable intrinsic parameters of these non-metric cameras impede good quality orthophoto productions. This paper presents an alternative method to measure the boundaries reliably without an existence of the orthophoto. A degraded quality of the orthophoto can be circumvented by our newly proposed method so called direct visual referencing. This method comprises two stages. The first step is to perform on the fly camera calibration to minimize instabilities of the intrinsic components of the non-metric camera. Modifying common and widely known flying paths for aerial photogrammetry mission is enabling a block variant self-calibrating bundle adjustments to proceed. The second step is a digitation process. Carefully selected Premark or prominent features along the boundaries are digitized on arbitrary selected images. These features are then matched to the similar ones onto all available images by performing multi photo geometrically constraint least squares image matching. Final results are 3D coordinates from the multi photos triangulation process. These boundaries coordinates are compared against the GPS-RTK measurements on the field. Deviations of these types of coordinates are around 1 cm. It is obvious that this method meets the precision requirement of the GPS-RTK measurements. Therefore we firmly believed that conducting UAV's cadastral surveys using direct visual referencing is very promising in the near future.

Keywords: UAV, Non-metric Camera, Cadaster, Precision, Calibration

1. Introduction

An orthophoto is defined as a differentially rectified image for presenting planimetric information only [1]. It provides valuable spatial and radiometric information in its true orthographic positions [2], and it is geometrically equivalent to maps which also show true orthographic positions of objects [3]. The absence of relief displacement and the uniform scale in orthophoto enable users to measure distances, compute areas, and perform terrain digitization. When dealing with large scale imagery over urban

areas such as images taken from a low altitude flying UAV, differential rectification produces a serious problem, i.e. ghosting effects, since the orthorectified images underwent a resampling process from the original image and might have been prepared from a low quality DEM which does not accurately model the ground surface [4]. The resulted orthophoto has lost some of its original resolution, therefore the accuracy may be degraded and horizontal errors within the orthophoto could be large [5]. Meanwhile orthophoto maps are believed by mapping communities as a favorable media to generate land parcel boundaries for cadaster survey related projects. Also, since burgeoning off-the-shelf cameras mounted on the UAV are commonly utilized for photographing such boundaries, unreliable and unstable intrinsic parameters of these non-metric cameras impede good quality orthophoto productions. This paper presents an alternative method to measure the boundaries reliably without an existence of the orthophoto. A degraded quality of the orthophoto can be circumvented by our newly proposed method so called direct visual referencing.

This method comprises two stages. The first step is to perform on the fly camera calibration to minimize instabilities of the intrinsic components of the non-metric camera. Modifying common and widely known flying paths for aerial photogrammetry mission is enabling a block variant self-calibrating bundle adjustments to proceed. The second step is a digitation process. Carefully selected Premark or prominent features along the boundaries are digitized on arbitrary selected images. These features are then matched to the similar ones onto all available images by performing multi photo least squares image matching. Both steps are elaborated as follows.

2. Methods

On the fly camera calibration means in-flight camera calibration utilizing convergent network geometry [6-10] to calibrate camera's intrinsic parameters with no existences of measured ground control points (GCPs). Due to Conventional flight configurations for aerial image acquisitions using small format cameras are uneconomic for the full provision of ground control points since each photograph covers a small area of ground [11], calibration are performed without necessarily measured GCPs on the field. Flight configurations are followed convergent network geometry to facilitate block invariant self-calibrating bundle adjustment model to calibrate the camera intrinsic parameters

[12] as well as determine object space coordinates of pre-marks' locations [13, 14]. The followings are general forms of the method in the form of Cayley matrix [15, 16]:

$$
\underset{(2mn,1)}{v_{ij}} = \underset{(2mn,6m)}{A1_{ij}} \underset{(6m,1)}{\delta1_i} + \underset{(2mn,3n)}{A2_{ij}} \underset{(3n,1)}{\delta2_j} + \underset{(2mn,p)}{A3_{ij}} \underset{(p,1)}{\delta3_p} - \underset{(2mn,1)}{l_{ij}}
\tag{1}
$$

Here i and j represent information pertaining to the ith image out of the m images and j^{th} object point out of the n object points; **v** is a vector of observational residuals in image coordinate measurements; **l** is a discrepancy term between approximation and observation; Δ1, Δ2 and Δ3 comprise corrections to starting values for the six exterior orientation parameters, three object space point coordinates (X, Y, Z) and p systematic error parameters; and **A**1, **A**2 and **A**3 are matrices of partial derivatives in terms of parameters. To recover the vectors Δ1 and Δ2 in the adjustment process, appropriate starting values for the parameters are required. The initial values for a spatial position and orientation of images are determined using a direct solution of space resection methods [17, 19] and relative orientation methods [20, 21], whereas a spatial position of the object space points are calculated by space intersection [22]. The generation of initial approximate values for all parameters is required in (1) because the photogrammetric observation equations are non-linear with respect to the parameters and must be iteratively solved using a linearized set of equations. The camera calibration stage occurs in the bundle adjustment computation which can be defined as a process of determining the exterior orientation of images with or without calibration parameters along with the object space point coordinates by utilizing least square adjustment process by observing measured image coordinates [23]. Based on (1) the normal equation for the bundle adjustment can be written as:

$$
\begin{bmatrix} A_1^T P A_1 & A_1^T P A_2 & A_1^T P A_3 \\ A_2^T P A_1 & A_2^T P A_2 & A_2^T P A_3 \\ A_3^T P A_1 & A_3^T P A_2 & A_3^T P A_3 \end{bmatrix} \begin{bmatrix} \delta1 \\ \delta2 \\ \delta3 \end{bmatrix} + \begin{bmatrix} A_1^T Pl \\ A_2^T Pl \\ A_3^T Pl \end{bmatrix} = 0
\tag{2}
$$

Where **P** is the weight matrix associated with the image coordinate measurements. Solutions of the normal equation of (2) are elaborated by [22, 24]. In the self-calibrating bundle adjustment process, provision of a fixed GCPs array on the calibration test field has no or little impact on the quality of the adjusted parameters. However, it requires the pre-mark's array be well distributed in three dimensions [13, 14] and it is necessary for a highly convergent imaging geometry for a recovery of the principal distance [15, 16] (i.e. calibrated focal length).

The important next step to enable the direct visual referencing to perform is that image matching which is a process to match corresponding points in digital images or parts thereof in the form of a reflectance level matrix [22, 25]. This research utilizes area-based method that based on a similarity on radiometric characteristics of pixels of grey values between corresponding points [25]. When having a point of feature in one image, its correspondence in the other one is computed by maximizing a certain similarity measure, defined over the grey value pixels within the image window. Two area based methods are employed namely a normalized cross correlation (CNN) and a least square image matching (LSM). The first method is required to approximate the matched patches to ensure a successful match by the latter one as depicted in Figure 1.
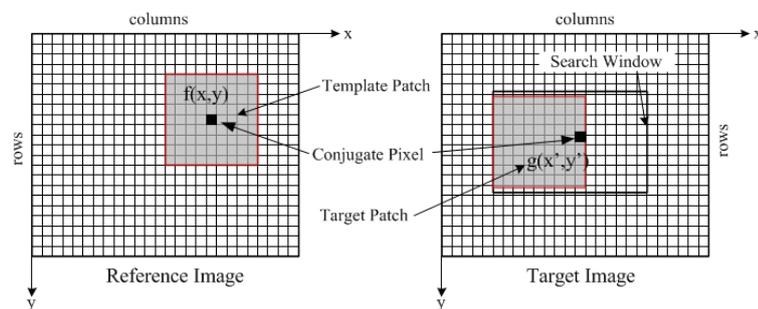

Figure 1: The concept of area-based matching.

A similarity measure of ρ is indicated by the NCC coefficient computed by comparing every pixel in the template patch on the reference image with the corresponding pixel in the target patch on the target image (Fig.1):

$$\rho = \sum_{y=1}^{row}\sum_{x=1}^{col}\left\{\left(f_{xy}-\overline{f}\right)\left(g_{xy}-\overline{g}\right)\right\} / \left\{\left(\sum_{y=1}^{row}\sum_{x=1}^{col}\left(f_{xy}-\overline{f}\right)^2\right)\left(\sum_{y=1}^{row}\sum_{x=1}^{col}\left(g_{xy}-\overline{g}\right)^2\right)\right\}^{1/2} \quad (3)$$

A col and row are the number of columns and rows of the patches respectively; the f_{xy} is y^{th} row the xth column of grey value from the template patch; the g_{xy} is y^{th} row the xth column of grey value from the target patch; the $\overline{f}$ and $\overline{g}$ are arithmetic mean of the grey values in template and target patch respectively [22, 25]. Major drawbacks of the NCC are that it does not take into account radiometric and geometric differences between patches, different lighting condition and high frequency noise contaminations [22, 25]. These disadvantages which need to account for geometric and radiometric differences between patches to optimize similarity measure are set up the context of least square estimation [25]. The LSM minimizes these differences while computing the position and reshaping the target patch during the least square estimation process [22, 26, 27]. It employs iterative geometric transformation and radiometric correction

between the template and target patch (Figure 1). The position and shape the target patch are both varied during the iteration until the differences between the patches reach a minimum [22, 28]. The template patch of f(x,y) with its row height and column width and the target patch of g(x,y) with an equal size are being matched, then the objective of the LSM is to estimate a new location of target patch g(x,y) on the target image such that the grey value differences between the template and the target are minimized. Thus, the standard parametric least squares adjustment for each pixel in the patches can be written as [25]:

$$f\left(x,y\right)-e\left(x,y\right) = g^0\left(x,y\right)+g_x da_{11}+g_x x_0 da_{12}+g_x y_0 da_{21}+g_y db_{11}$$
$$+g_y x_0 db_{12}+g_y y_0 db_{21}+r_s+r_t g^0\left(x,y\right) \tag{4}$$

Where e(x,y) is a goal function of the true error vector which measures the differences on both patches. The position and reshaping parameters are $da_{11}, da_{12}, da_{21}, db_{11}, db_{12}, db_{21}$, whereas radiometric parameters are the shift r_s and the scale r_t of grey values, applied to the target patch. Once the conjugate point was found on the overlapping images, the final step is to calculate the point on ground surface by intersecting the conjugate points. While the intrinsic and extrinsic parameters are computed from the self-calibrating bundle adjustment process, the object space points of land parcel boundaries are determined from the space intersection of the (1):

$$\begin{matrix} v_{ij} \\ (2mn,1) \end{matrix} = \begin{matrix} A2_{ij} \\ (2mn,3n) \end{matrix} \begin{matrix} \delta2_j \\ (3n,1) \end{matrix} - \begin{matrix} l \\ (2mn,1) \end{matrix} \tag{5}$$

The vector $\delta2$ can be computed iteratively based on (2). Since the remaining unknowns in (5) are the correction to be applied to initial approximation for the object space point, they are added to the initial values of that particular point.

3. Result and Discussion

In this research, a pocket size camera of Nikon 12MP Coolpix P300 with a focus of around 6mm is mounted on the multi-rotor UAV based acquisition platform. The camera sensor size of 1/2.3 inch (i.e. 7.66mm x 6.17mm) and image size of 4000x3000 pixels produces images with varying ground sampling distance of about 16mm to 20mm. A test area of around 1.5 Hectares is photographed twice (Fig.2a). First, a nadir view looking camera is set up to capture vertical images. Then a viewing direction of the camera is directed approximately at 40 degrees off nadir view to capture oblique images. A convergent flight configuration is performed by circling an Area of Interest at the middle of the test

area. Both the vertical and oblique images constitute about 150 photos and some of them are illustrated in Fig.2b.
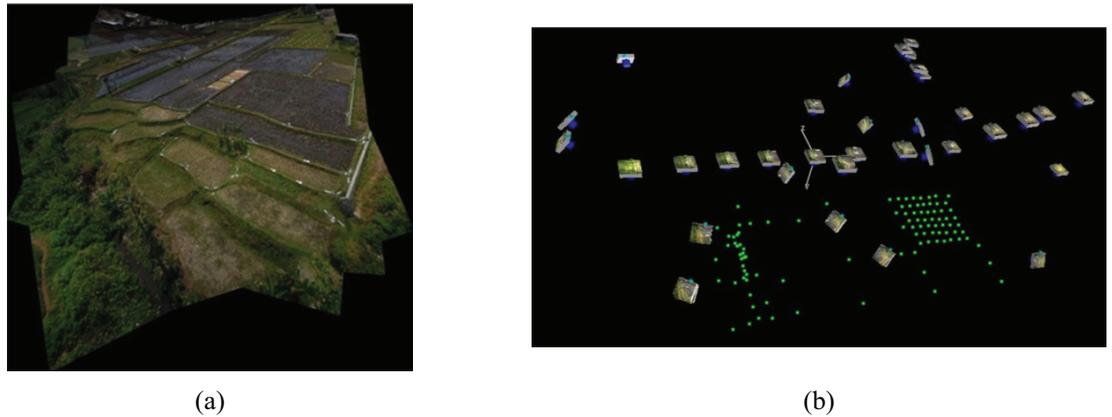

(a)   (b)

Figure 2: (a). Topography of the test area consists of wet and dry paddy field with moderate vertical slopes, (b). Some of the captured vertical images and convergent oblique images photograph the Area of Interest (green dots).

To precede the self-calibrating bundle adjustment process, an array of 7 x 7 retro targets spaced of about 8m as well as a number of retro targets placement along the parcel boundaries are arranged (e.g. green dots on Fig.2b). For quick identification purposes these retro targets are surrounded by Premark, except for the array in the calibration area (Figure 2a, Figure 3a, and Figure 3b). The bundle adjustment computation is performed using proprietary photogrammetric software to determine the exterior orientation (EO) parameters of each image together with the camera's intrinsic parameters shown in Table 1.

(a)   (b)

Figure 3: (a). Retro target and Premark seen from the vertical image, (b). The array of retro targets without Premark in the calibration area seen from the oblique image.

Once the camera's intrinsic parameters as seen in Table 1 and the EO parameters of each image computed, the next step is to digitize the boundary of the parcels. The digitization process realize as if it traces feature boundaries in the object space through a provision of the overlapping images. In other words, a selected feature along the

Table 1: Nikon Coolpix P300 Intrinsic parameters resulting from the self-calibrating bundle adjustment computations.

Focal length & Principal point (mm)		Radial distortion		Decentering distortion		Linier distortion	
c:	5.8315	K1:	1.3081e-003	P1:	-4.8755e-004	B1:	0.0680
xp:	0.0883	K2:	-2.7693e-005	P2:	6.1688e-004	B2:	0.0017
yp:	-0.1058	K3:	9.7972e-007	-	-	-	-

boundary lines on one image could be triangulated by matching the conjugate features on other overlapping images. This situation can be explained from Fig.4 as follows.
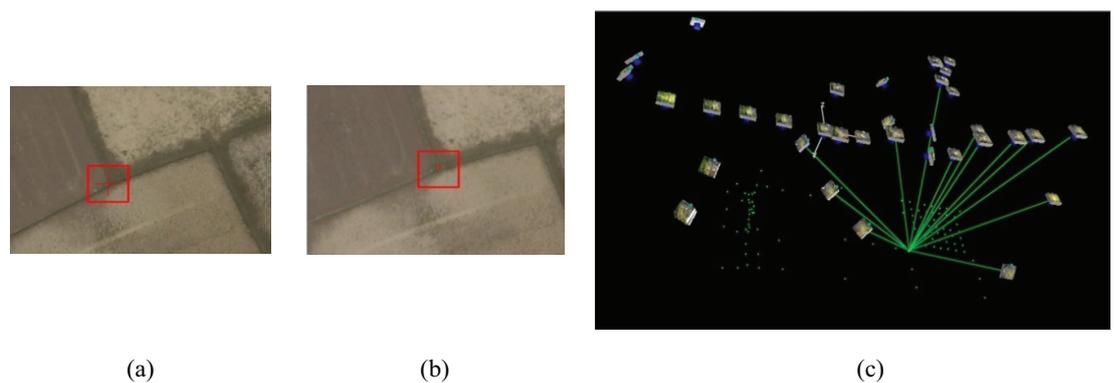

| (a) | (b) | (c) |

Figure 4: (a). Template patch, (b). Target patch, (c). A conjugate point seen from overlapping images.

If a boundary feature is selected by a mouse click, the selected patch would be regarded as a template patch (Figure 4a). By utilizing the known EO parameters of each image, the conjugate feature on other overlapping images can be found by employing the CNN and the LSM matching simultaneously [25] through imposing an epipolar line constraint or a vertical line locus constraint [22]. A matched conjugate feature on other image is illustrated in Figure 4b. All founded conjugate features on all overlapping images (Figure 4c) proceed to a triangulation computation to determine its object space coordinates. This process is repeated interactively to delineate all desired parcel boundaries in the object space. A tangible benefit of this method is that the extracted boundaries are expressed in terms of 3D coordinates, and the influences of lens distortion can be minimized. Furthermore, no orthophoto or orthophoto maps are needed for the delineation process.

To test a reliability of the method, a field test was conducted to measure the boundaries features twice using GPS-RTK measurements and Total Station for obtaining doubtless reliable coordinates. Every centroid of the retro targets along the parcel boundaries is observed (Figure 5a and Figure5b). The very same retro targets are observed on the images using aforementioned method. Hence this strategy ensures the same features on the ground and on the images are observed. A reason to choose

a white circle retro target surrounded by dark background is to provide very precise centroid determination [29, 30] which up to 0.01 pixel.
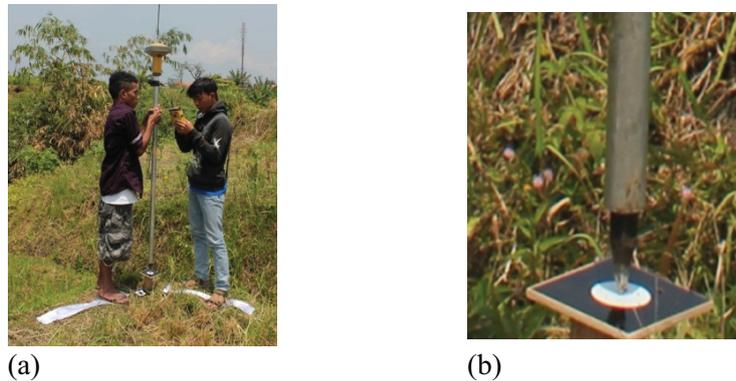

(a)   (b)

Figure 5: (a). Coordinate measurement of retro target using GPS-RTK, (b). Centroid of the retro target observation

To ascertain a determination of parcel area using this method, we compare the area obtained from the GPS-RTK observations and the one obtained from an orthophoto map generated from proprietary photogrammetric software. The results are presented in Table 2 as follows.

TABLE 2: Analysis of parcel area differences from three methods.

Parcel Label	Area from GPS-RTK (m^2)	Area from Orthophoto map (m^2)	Area from our method (m^2)	Area discrepancies (m^2) (from GPS-RTK & orthophoto map)	Area discrepancies (m^2) (from GPS-RTK & our method)
A1	487.05	499.482	487.048	12.432	0.002
A2	314.68	324.891	314.679	10.211	0.001
A3	446.83	461.080	446.827	14.250	0.003
A4	289.592	305.074	289.339	15.482	0.253
A5	187.979	208.663	187.486	20.684	0.493
A6	37.667	49.654	37.666	11.987	0.001
A7	113.751	128.209	113.608	14.458	0.143

The GPS-RTK observation in the Table 2 is the benchmark for the analysis of the parcel area. The coordinates obtained from the GPS-RTK observation as well as the ones from our method are used to calculated parcel area. However, the areas from the orthophoto map are obtained by digitizing the retro targets on the orthophoto map directly. From the area deviation data, it is clearly show that our method meet the accuracy requirements of the GPS-RTK to delineate the parcel boundaries rather than that of using the orthophoto map which give the average discrepancies of about 0.128m^2. Our direct visual referencing method is equal in precision with the GPS-RTK

ones as long as the vertical and oblique images are available and the camera's intrinsic parameters are solved for the aerial convergence network.

4. Conclusions

The direct visual referencing method is very promising for conducting UAV's cadastral survey since it meets the accuracy requirement of the GPS-RTK observation. The very promising results are made through a provision of the multi images least squared image matching and multi images triangulation methods from the interactively selected features on images which are free from lens distortion influences. We hope that this finding could be an acceptable method for parcel boundaries delineations using UAV in the near future.

Acknowledgment

References

[1] T. J. Blachut and M. C. Van-Wijk, Photogramm. Eng. **36**, 365--374 (1970).

[2] K. I. Bang and A. F. Habib, ``Comparative analysis of alternative methodologies for true ortho-photo generation from high resolution satellite imagery,'' in *ASPRS 2007 Annual Conference*, (ASPRS, Florida, 2007), p 12.

[3] P. Wolf, B. Dewitt, and E. Mikhail, *Elements of Photogrammetry with Applications in GIS* 3rd ed. (McGraw-Hill Companies Inc., New York, 2000), pp. 301 - 303.

[4] J. C. McGlone, *Manual of Photogrammetry: 6th Edition* (American Society for Photogrammetry and Remote Sensing, Bethesda-Maryland, 2013), p.1318.

[5] C. A. Rokhmana, I. A. Gumeidhidta, and M. E. Tjahjadi, ``Potential use of uav-based mapping system to accelerate the production of parcel boundary map in Indonesia,'' in *The 1st International Conference on Geodesy, Geomatics, and Land Administration 2019*, AIP Conference Proceeding, (Accepted).

[6] J. M. Anderson and C. E. Lee, Photogramm. Eng. Remote Sens. **41**, 1337--1348 (1975).

[7] E. Honkavaara, *Int. Arch.* Photogramm. Remote Sens. Spat. Inf. Sci. **35**, 166--172 (2004).

[8] G. Konecny, Photogrammetria **22**, 37--57 (1967).

[9] S. O. Mason, Photogramm. Rec. 15, 277--299 (1995).

[10] Y. I. Abdel-Aziz, Photogramm. Eng. 45, 1141--1346 (1974).

[11] W. S. Warner and L. E. Blankenberg, Photogramm. Rec. 15, 217--224 (1995).

[12] M. R. Shortis, S. Robson, and H. A. Beyer, Photogramm. Rec. 16, 165--186 (1998).

[13] M. E. Tjahjadi, S. S. Sai, and C. A. Rokhmana, ``Assessing stability performance of non-metric camera's lens distortion model during uav flight missions,'' in The 1st International Conference on Geodesy, Geomatics, and Land Administration 2019, AIP Conference Proceeding, (Accepted).

[14] M. E. Tjahjadi, S. S. Sai, and F. Handoko, ``Assessing a 35mm fixed-lens sony alpha-5000 intrinsic parameters prior to, during, and post uav flight mission,'' in The 1st International Conference on Geodesy, Geomatics, and Land Administration 2019, AIP Conference Proceeding, (Accepted).

[15] C. S. Fraser, ``Photogrammetric Camera Component Calibration: A review of Analytical Technique,'' in Calibration and Orientation of Cameras in Computer Vision, edited by A. W. Gruen and T. S. Huang (Springer-Verlag, Berlin Heidelberg, 2010), pp. 93--121.

[16] T. Luhmann, C. Fraser, and H. G. Maas, ISPRS J. Photogramm. Remote Sens. 115, 37--46 (2016).

[17] M. E. Tjahjadi, ARPN J. Eng. Appl. Sci. 11, 3449--3455 (2016).

[18] M. E. Tjahjadi and F. Handoko, ``Single frame resection of compact digital cameras for UAV imagery,'' in Deep Learning High Speed Processing technologies and Its Application on Electrical, Electronics, Computer science and Informatics for Humanity, 4th International Conference on Electrical Engineering, Computer Science and Informatics (EECSI), edited by M. A. Riyadi et al. (IEEE, Yogyakarta, 2017), pp. 409-413.

[19] M. E. Tjahjadi and F. D. Agustina, ``Single image orientation of UAV's imagery using orthogonal projection model,'' in Achieving Sustainability through Digital Earth, 2017 International Symposium on Geoinformatic (ISyG), (IEEE, Malang, 2017), pp.19-24.

[20] M. E. Tjahjadi and F. D. Agustina, ``A Relative Rotation between Two Overlapping UAV's Images,'' in Toward the Next Generation of technology, 5th International Conference on Electrical Engineering, Computer Science and Informatics (EECSI), edited by A. Yudhana et al. (IEEE, Malang, 2018), pp. 658--663.

[21] M. E. Tjahjadi and F. D. Agustina, Int. J. Adv. Intell. Informatics 5, 1, 24--39 (2019).

[22] M. E. Tjahjadi, NURBS Reconstruction in Object Space from Stereo Images: A Photogrammetric Approach (LAP LAMBERT Academic Publishing GmbH & Co. KG, Saarbucken Deutschland, 2010), pp.5 -- 50.

[23] B. Triggs, P. F. McLauchlan, R. I. Hartley, and A. W. Fitzgibbon, Lecture Notes in Computer Science 1883, 298--372 (2000).

[24] H. Wolf, ``The Helmert Block Method-Its Origin and Development,'' in Proceedings of the Second International Symposium on Problems Related to the Redefinition of North American Geodetic Networks, (NOAA, Arlington-Va,1978), pp. 319--326.

[25] M. E. Tjahjadi and F. Handoko, ``Precise wide baseline stereo image matching for compact digital cameras,'' in Deep Learning High Speed Processing technologies and Its Application on Electrical, Electronics, Computer science and Informatics for Humanity, 4th International Conference on Electrical Engineering, Computer Science and Informatics (EECSI), edited by M. A. Riyadi et al. (IEEE, Yogyakarta, 2017), pp. 181- 186.

[26] H. Bischof and F. Leberl, ``Digital Image Processing,'' in Manual of Photogrammetry: 6th Edition, edited by J. C. McGlone (American Society for Photogrammetry and Remote Sensing, Bethesda -- Maryland, 2013), pp. 451--515.

[27] A. Irscharaa, M. Rumplerb, P. Meixnerb, T. Pockb, and H. Bischof, ISPRS Annals of the Photogrammetry, Remote Sensing and Spatial Information Sciences, I--3, 227--232, (2012).

[28] Mayer, M. Sester, G. Vosselman, and G. Y. G. Lee, ``Basic Computer Vision Technique,'' in Manual of Photogrammetry 6th Edition, edited by J. C. McGlone (American Society for Photogrammetry and Remote Sensing, Bethesda -- Maryland, 2013), pp. 517--583.

[29] H. L. Mitchell and L. J. Pilgrim, ``Selection of an Image Matching Algorithm,'' in Symposium on the Application of Close Range Photagrametry, (1987), pp. 23--31.

[30] J. C. Trinder, T. Tjugiarto, and B. E. Donnelly, Aust. J. Geod. Photogramm. Surv. 53, 1--13 (1990).